

Discovery of Diffuse Hard X-Ray Emission from the Vicinity of PSR J1648–4611 with Suzaku

Michito SAKAI,¹ Hironori MATSUMOTO,² Yoshito HABA,² Yasufumi KANOU,¹ and Youhei MIYAMOTO¹

¹*Division of Particle and Astrophysical Science, Graduate School of Science, Nagoya University, Furo-cho, Chikusa-ku, Nagoya 464-8602*
m_sakai@u.phys.nagoya-u.ac.jp

²*Kobayashi-Maskawa Institute for the Origin of Particles and the Universe, Nagoya University, Furo-cho, Chikusa-ku, Nagoya 464-8602*

(Received ; accepted)

Abstract

We observed the pulsar PSR J1648–4611 with Suzaku. Two X-ray sources, Suzaku J1648–4610 (Src A) and Suzaku J1648–4615 (Src B), were found in the field of view. Src A is coincident with the pulsar PSR J1648–4611, which was also detected by the Fermi Gamma-ray Space Telescope. A hard-band image indicates that Src A is spatially extended. We found point sources in the vicinity of Src A by using a Chandra image of the same region, but the point sources have soft X-ray emission and cannot explain the hard X-ray emission of Src A. The hard-band spectrum of Src A can be reproduced by a power-law model with a photon index of $2.0^{+0.9}_{-0.7}$. The X-ray flux in the 2–10 keV band is 1.4×10^{-13} erg cm⁻² s⁻¹. The diffuse emission suggests a pulsar wind nebula around PSR J1648–4611, but the luminosity of Src A is much larger than that expected from the spin-down luminosity of the pulsar. Parts of the very-high-energy γ -ray emission of HESS J1646–458 may be powered by this pulsar wind nebula driven by PSR J1648–4611. Src B has soft emission, and its X-ray spectrum can be described by a power-law model with a photon index of $3.0^{+1.4}_{-0.8}$. The X-ray flux in the 0.4–10 keV band is 6.4×10^{-14} erg s⁻¹ cm⁻². No counterpart for Src B is found in literatures.

Key words: acceleration of particles — X-rays: individual (PSR J1648–4611, HESS J1646–458)

1. Introduction

The HESS (High Energy Stereoscopic System) Collaboration has recently reported the detection of the degree-scale extended very-high-energy (VHE) γ -ray source HESS J1646–458 (Abramowski et al. 2012). The VHE γ -ray source is centered on the massive stellar cluster Westerlund 1 (Westerlund 1961). Abramowski et al. (2012) proposed two scenarios. One is a single-source scenario, where Westerlund 1 is favored as site of VHE particle acceleration. Here, a hadronic parent population would be accelerated within the stellar cluster. The other is a multi-source origin, where a scenario involving the pulsar PSR J1648–4611 (Kramer et al. 2003) could be viable to explain parts of the VHE γ -ray emission of HESS J1646–458.

PSR J1648–4611 is a radio pulsar discovered by the Parkes Multibeam Pulsar Survey (Kramer et al. 2003). It is located at the position $(l, b) = (339^\circ.4383, -00^\circ.7938)$ ¹ with a pulse period of $P = 0.1649$ s and a period derivative of $\dot{P} = 23.7 \times 10^{-15}$ s s⁻¹. The distance to the source was estimated to be $d = 5.7$ kpc from the pulsar’s dispersion measure using the Taylor & Cordes (1993) model for the Galactic distribution of free electrons. The characteristic age and the spin-down luminosity are $\tau_c = 1.1 \times 10^5$ yr and $\dot{E} = 2.1 \times 10^{35}$ erg s⁻¹, respectively.

Recently, the Large Area Telescope (LAT) on the Fermi Gamma-ray Space Telescope (Fermi) detected γ -ray source that is spatially associated with the PSR J1648–4611 (2FGL J1648.4–4612; Nolan et al. 2012). A γ -ray pulse detection from this pulsar is also reported in the Public List of LAT-Detected Gamma-Ray Pulsars.² These results imply that the origin of the VHE γ -ray emission also relates to this pulsar. Active pulsars are losing a significant part of energy via relativistic particles, and form pulsar wind nebulae (PWNe). PWNe emit synchrotron emission from the radio to X-ray bands. In addition, some PWNe are known to be VHE γ -ray emitters. Thus, PSR J1648–4611 is a possible candidate for the source of the energy of HESS J1646–458. However, X-ray emission from PSR J1648–4611 has not been reported.

In the following sections, the results of the Suzaku observation of PSR J1648–4611 will be discussed; in addition, our own analysis on the Chandra observation of this region will be utilized to estimate the contribution of point sources. In this paper, uncertainties are described at the 90% confidence level, while the errors of data points in X-ray spectra and radial profiles are at the 1σ level, unless otherwise stated.

¹ $(\alpha, \delta)_{J2000.0} = (16^{\text{h}}48^{\text{m}}22^{\text{s}}.0, -46^\circ11'16''.0)$.

² See <https://confluence.slac.stanford.edu/display/GLAMCOG/Public+List+of+LAT-Detected+Gamma-Ray+Pulsars>).

2. Observations and Data Reduction

2.1. *Suzaku*

We observed the PSR J1648–4611 region with *Suzaku* (Mitsuda et al. 2007) on 2010 September 23 and 24 (OBSID=505051010). The observation was performed with the three CCD cameras (XISs: Koyama et al. 2007) located in the focal planes of the X-ray telescopes (XRTs: Serlemitsos et al. 2007) and the non-imaging detector (HXD: Kokubun et al. 2007; Takahashi et al. 2007). One of the XIS sensors (XIS 1) has a back-illuminated (BI) CCD, while the other two (XISs 0 and 3) utilize front-illuminated (FI) CCDs. Because one of the FIs (XIS 2) suffered catastrophic damage on 2006 November 9, no useful data were obtained. The XIS was operated in the normal clocking mode (without the Burst or Window options) with Spaced-row Charge Injection (SCI) (Uchiyama et al. 2009).

We analyzed the data with the processing version of 2.5.16.28,³ utilizing the HEADAS software (version 6.11.1) and calibration database (CALDB) released on 2011 November 10. All data affected by the South Atlantic Anomaly and telemetry saturation were excluded. We excluded the data obtained with an elevation angle from the Earth rim of $< 5^\circ$. Additionally, for the XIS data, we also excluded the data obtained with that from the bright Earth rim of $< 20^\circ$ and removed hot/flickering pixels. After these data screenings, the effective exposure for the XIS data was 50.2 ks, and that for the HXD data was 40.8 ks. In this paper, we concentrate on the XIS data.

2.2. *Chandra*

Chandra observed the PSR J1648–4611 region on 2010 January 24 (OBSID=11836). The exposure time was 10.2 ks. *Chandra* has a superior angular resolving capability. We analyzed *Chandra* data in order to estimate the contribution of point sources and the intensity upper limit of an undetected source, using the *Chandra* Interactive Analysis of Observations (CIAO) software version 4.3.1 with CALDB version 4.4.6.

3. Analysis and Results

3.1. *Images*

We extracted XIS images in the soft- and hard-energy bands from each sensor using the screened data. For the FI sensors, the soft- and hard-bands are defined as 0.4–3 keV and 3–10 keV, respectively, while those for the BI sensor are defined as 0.3–3 keV and 3–7 keV, respectively. The corners of the CCD chips illuminated by the ^{55}Fe calibration sources were excluded. Non-X-ray backgrounds (NXB) generated with `xisnxbgen` (Tawa et al. 2008) were subtracted from the images. Then, the soft- and hard-band images were divided by flat sky

³ See (<http://www.astro.isas.jaxa.jp/suzaku/process/history/v251628.html>).

images simulated at 1.49 and 4.5 keV using the XRT+XIS simulator `xissim` (Ishisaki et al. 2007) for vignetting corrections. The images were binned by a factor of 8. The images from the two FI sensors were summed.

Figure 1 shows the XIS FI images of the PSR J1648–4611 region smoothed using a Gaussian function with $\sigma = 0'.28$. The XIS BI images were essentially the same, except for the poorer statistics. In the hard-band image, an X-ray source with a peak position of $(l, b) = (339^\circ.44, -0^\circ.79)$ ⁴ was found, and was designated as Suzaku J1648–4610 (Src A). The peak position of Src A is close to PSR J1648–4611. The spatial distribution of Src A in the soft-band image seems to be different from that in the hard-band image (Figures 1(a) and (b)). The peak position in the soft-band image is $(l, b) = (339^\circ.44, -0^\circ.78)$ ⁵, and is close to Src 1 found in a Chandra image (see the end of section 3.1).

Another X-ray source, found at $(l, b) = (339^\circ.42, -0^\circ.90)$ ⁶, was also bright in the soft X-ray band. We designated this source as Suzaku J1648–4615 (Src B). Src B was not conspicuous in the hard-band image.

We created a radial profile of Src A in the 3–10 keV band as shown in Figure 2, and the profile was compared with a point-spread function (PSF). The origin of the radial profile was the peak in the hard-band image. As for the PSF, we obtained the radial profile using the SS Cyg data observed on 2005 November 2 (OBSID=400006010), which are the verification phase data for the imaging capability of the XRT (Serlemitsos et al. 2007). Since the energy dependence of the PSF is negligible (Serlemitsos et al. 2007), the radial profile was extracted from the 0.4–10 keV band. In this analysis, the NXB subtraction and vignetting correction were not applied to both the radial profiles of Src A and the PSF. As shown in Figure 2, the profile cannot be fitted adequately with the PSF plus a constant component model ($\chi^2/d.o.f. = 146.1/48$), and therefore Src A must be diffuse emission or unresolved multiple sources.

Figure 3 shows the Chandra image around Src A in the 0.4–10 keV band. Several sources can be seen around Src A. A point source search was carried out in the image with `wavdetect`. This tool uses a wavelet method (Freeman et al. 2002). The wavelet scales of `wavdetect` were the $\sqrt{2}$ series: 1.0 1.414 2.0 2.828 4.0 5.657 8.0 11.314 16.0. The threshold significance was set to 10^{-6} , this is equivalent to stating that the expected number of false sources per the ACIS-I3 CCD chip is one. We resolved 5 point sources from the whole region of the ACIS-I3 CCD chip. Their positions and counts are listed in table 1. The detected point sources around Src A are indicated by solid circles with the source numbers in figure 3. From the SIMBAD Astronomical Database operated at CDS, Strasbourg, France, we found a counterpart of Src 1 at $(l, b) = (339^\circ.4396, -00^\circ.7792)$ ⁷, which is an A0 Star: HD 151228.

⁴ $(\alpha, \delta)_{J2000.0} = (16^{\text{h}}48^{\text{m}}20^{\text{s}}, -46^\circ10'57'')$.

⁵ $(\alpha, \delta)_{J2000.0} = (16^{\text{h}}48^{\text{m}}18^{\text{s}}, -46^\circ10'32'')$.

⁶ $(\alpha, \delta)_{J2000.0} = (16^{\text{h}}48^{\text{m}}45^{\text{s}}, -46^\circ15'57'')$.

⁷ $(\alpha, \delta)_{J2000.0} = (16^{\text{h}}48^{\text{m}}18^{\text{s}}.4, -46^\circ10'38''.5)$.

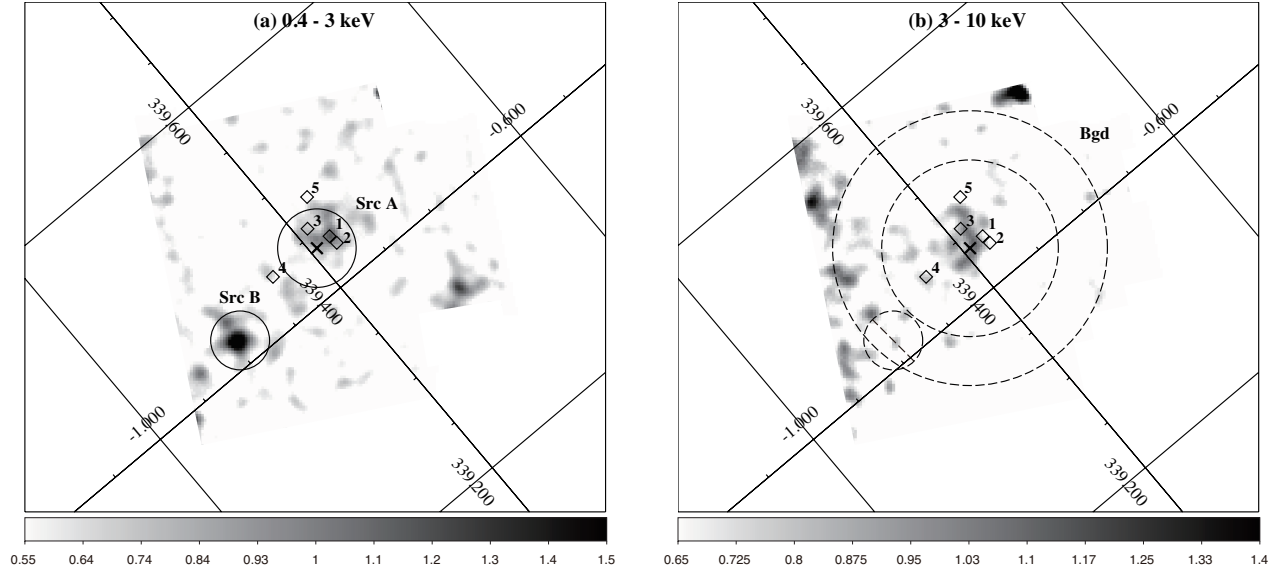


Fig. 1. Suzaku XIS FI (XIS 0+3) images of the PSR J1648–4611 region in the Galactic coordinates: (a) 0.4–3 keV and (b) 3–10 keV bands. The images were smoothed using a Gaussian function with $\sigma = 0'.28$. A vignetting correction was applied after subtracting the NXB, as described in the text. The cross mark represents the position of PSR J1648–4611. The numbered diamond points mark the Chandra point sources, whose properties are listed in table 1. The source regions for the spectrum of Src A and Src B are shown by the solid circles. The background region is shown by the dashed annulus excluding the source region of Src B.

Table 1. Chandra point sources around the field of PSR J1648–4611.

Source numbers	<i>RA</i> (J2000.0)	<i>Dec</i> (J2000.0)	Counts* (0.4 – 10 keV)
Src 1	16 48 18.30	-46 10 39.4	26 ± 5
Src 2	16 48 16.16	-46 10 59.7	7 ± 3
Src 3	16 48 24.78	-46 10 16.6	8 ± 3
Src 4	16 48 34.95	-46 12 43.7	4 ± 2
Src 5	16 48 24.91	-46 08 39.6	3 ± 2

* The sum of all counts in the source cell minus the sum of the estimated background counts.

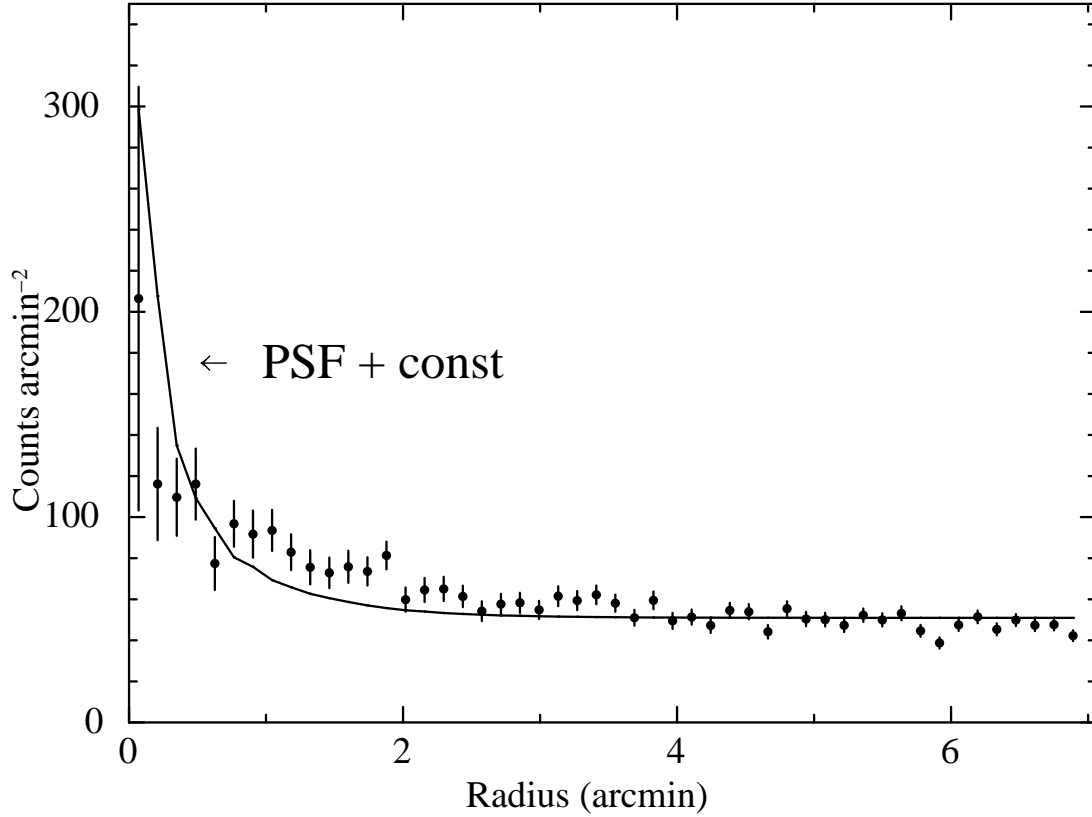


Fig. 2. Radial profile of Src A extracted from the 3–10 keV band image of the XIS FI sensor (XIS 0+3). The solid line represents the XIS PSF profile with a constant component.

3.2. Spectra

3.2.1. Src A

An X-ray spectrum of Src A of each XIS sensor was extracted from a circular region with a radius of $2'$. An annulus region with an inner radius of $4.5'$ and an outer radius of $7'$ was used for a background spectrum. NXB spectra in the source and background regions were constructed using `xisnxbgen` (Tawa et al. 2008), and the NXB were subtracted from the source and background spectra. When the background spectrum was subtracted from the source spectrum, a vignetting correction was taken into account. The spectra of Src A thus obtained are shown in figure 4. In the spectrum analysis below, Redistribution Matrix Files (RMFs) and Ancillary Response Files (ARFs), made using the softwares `xisrmfgen` and `xissimarfgen` (Ishisaki et al. 2007), were used.

The Chandra image (figure 3) shows that the Src A region includes three point sources. A Chandra spectrum including all three sources was constructed in order to estimate the contribution of the point sources to the Suzaku spectra. Circular regions with a radius of $3''.4$

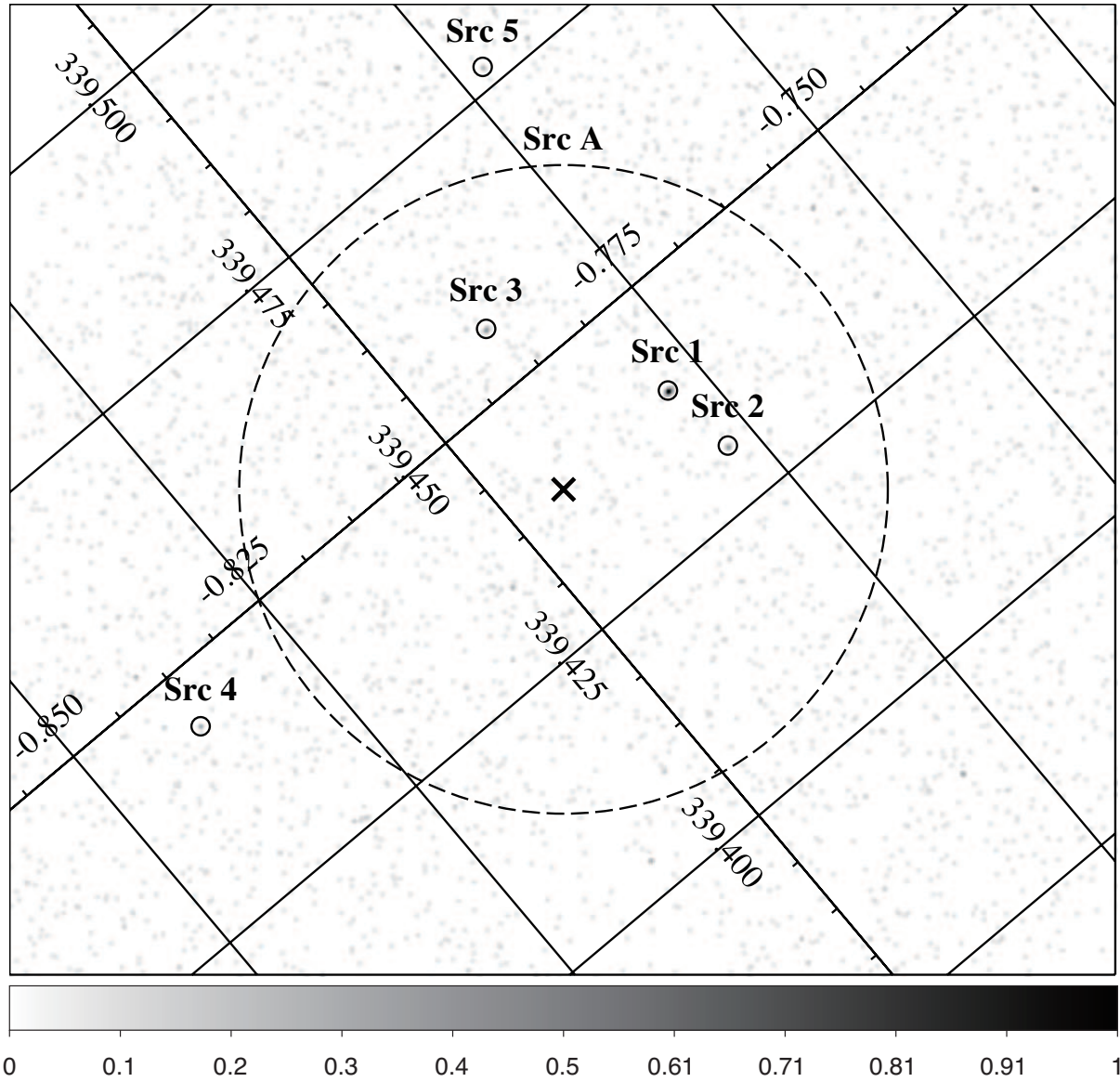


Fig. 3. Chandra image around PSR J1648–4611 in the 0.4–10 keV band including the XIS source region for Src A (dashed circle). Point sources are indicated by solid circles with the source numbers. Src 1 is coincident with HD 151228. The cross mark represents the position of PSR J1648–4611. Lines of constant Galactic latitude and longitude are plotted and labeled in the interior of the figure.

centered on each source were used for the source spectrum, and annular regions with an inner radius of $5''$ and an outer radius of $12''6$ around each source were used for a background spectrum. The spectrum thus obtained (figure 5) is soft where almost no X-ray photon can be seen above 2 keV. Note that the Suzaku soft-band image seems to follow the distribution of the Chandra point sources, while the hard-band image shows a different distribution (figure 1). This suggests that the soft emission of Src A is attributed to the Chandra sources and that the origin of the hard emission of Src A is different from that of the soft emission. We fitted a bremsstrahlung model with interstellar absorption to the Chandra spectrum of point sources in the 0.4–2 keV band. The cross sections of the photoelectric absorption were obtained from Morrison & McCammon (1983). A hydrogen-equivalent column density N_{H} , plasma temperature kT , and a normalization were set to be free parameters. The best-fit parameters are $N_{\text{H}} = 0.1_{-0.1}^{+0.7} \times 10^{22} \text{ cm}^{-2}$ and $kT = 0.45_{-0.28}^{+0.60} \text{ keV}$, and $\chi^2/d.o.f.=5.99/15$. The observed flux in the 0.4–2 keV band is $F(0.4\text{--}2 \text{ keV}) = (3.4 \pm 1.0) \times 10^{-14} \text{ erg cm}^{-2} \text{ s}^{-1}$.

The Suzaku spectra of Src A in the 0.4–2 keV band were compared with simulated spectra of the Chandra sources within the Src A region. In the simulation, we took into account the leakage of photons from Srcs 1, 2, and 3, and the contamination from Srcs 4 and 5. Since the count rates of Srcs 4 and 5 were quite small (table 1), a qualitative analysis of the combined spectrum of Srcs 4 and 5 was impossible. We assume that Srcs 4 and 5 have the same spectral shape as the best-fit model to the Chandra Srcs 1, 2, and 3. The count rates of the Chandra sources were varied, but the ratios between them were fixed according to the values in table 1. We found that the Suzaku spectra in the 0.4–2 keV band can be explained ($\chi^2/d.o.f = 20.37/15$) when the total flux of the Chandra Srcs 1, 2, and 3 is $(2.6 \pm 1.3) \times 10^{-14} \text{ erg cm}^{-2} \text{ s}^{-1}$ (figure 6). This value is consistent with the above Chandra result of $(3.4 \pm 1.0) \times 10^{-14} \text{ erg cm}^{-2} \text{ s}^{-1}$, and it is reasonable to conclude that the Suzaku soft-band spectra of Src A can be explained by the Chandra point sources.

On the other hand, the Suzaku spectra of Src A in the 2–10 keV band cannot be described by the Chandra point sources alone having soft X-ray emission. In the model fitting of the Suzaku spectra of Src A in the 0.4–10 keV band, we added a power-law component modified by interstellar absorption to explain the remaining hard X-ray emission. A hydrogen column density (N_{H}), a photon index (Γ), and a normalization were free parameters. The spectra of Src A with the best-fit model are shown in figure 6; the best-fit parameters are $N_{\text{H}} = 3.4_{-1.6}^{+2.4} \times 10^{22} \text{ cm}^{-2}$, $\Gamma = 2.0_{-0.7}^{+0.9}$, and $\chi^2/d.o.f.=60.49/55$. The observed flux of the power-law component in the 2–10 keV band is $F(2\text{--}10 \text{ keV}) = 1.4 \times 10^{-13} \text{ erg cm}^{-2} \text{ s}^{-1}$. The contribution of point sources is indicated by the dotted lines in the soft-band. The additional dotted lines in the hard-band show the power-law model.

3.2.2. Src B

The Suzaku spectra of Src B were extracted from a circular region centered on Src B. We found no counterpart for Src B in literatures. A circle with a radius of 1.5 is used as

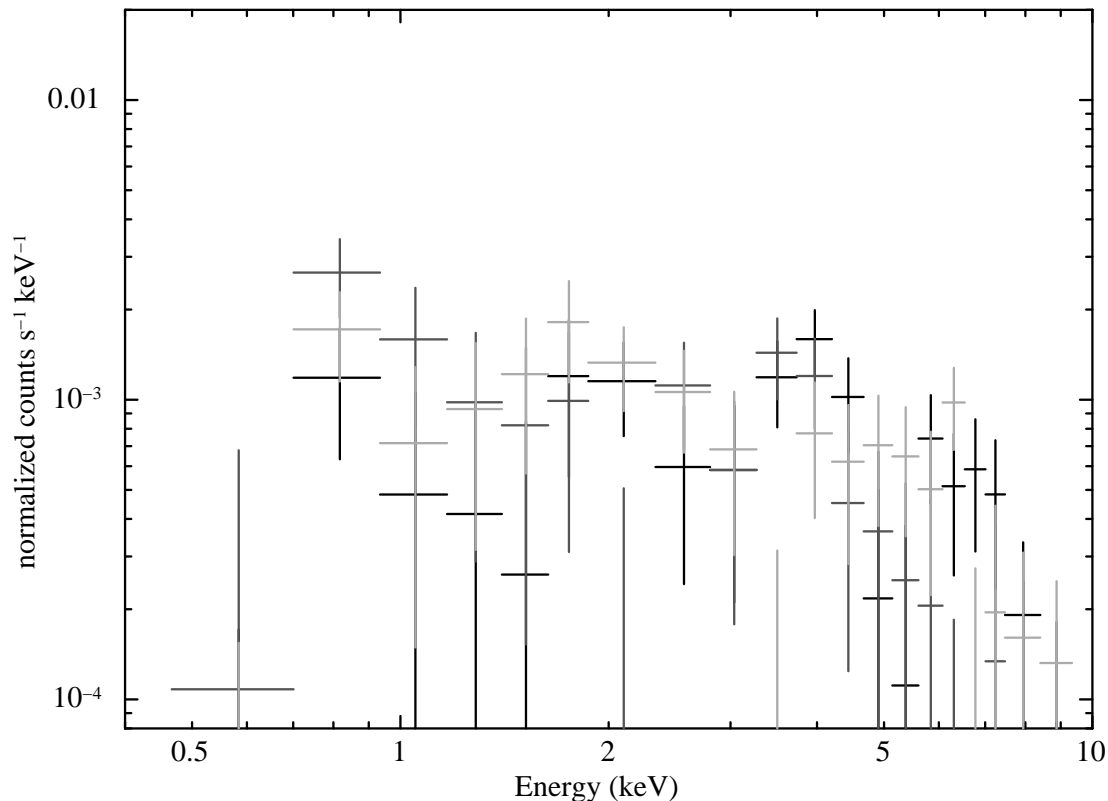


Fig. 4. XIS spectra of Src A. Black, Dark Gray and Light Gray lines represent the data for the XIS0, XIS1 and XIS3, respectively.

the source region and an annulus with an inner radius of $4'5$ and an outer radius of $7'$ is used for the background. The spectra of Src B are shown in figure 7. We fitted the spectra with an absorbed power-law model. The best-fit parameters are $N_{\text{H}} = 0.3_{-0.2}^{+0.3} \times 10^{22} \text{ cm}^{-2}$, $\Gamma = 3.0_{-0.8}^{+1.4}$, and $\chi^2/d.o.f. = 29.88/31$. The observed flux in the 0.4–10 keV band is $F(0.4\text{--}10 \text{ keV}) = 6.4 \times 10^{-14} \text{ erg cm}^{-2} \text{ s}^{-1}$.

We also tried to fit an absorbed thermal plasma model (the APEC model: Smith et al. 2001). The thermal model yields a hydrogen column of zero ($< 1.0 \times 10^{22}$) cm^{-2} , a temperature of $1.9_{-1.3}^{+1.1}$ keV, an abundance of 0.26 (< 1.03) solar, and $\chi^2/d.o.f. = 28.73/30$. The observed flux in the 0.4–10 keV band is $F(0.4\text{--}10 \text{ keV}) = 6.4 \times 10^{-14} \text{ erg cm}^{-2} \text{ s}^{-1}$.

3.3. Intensity upper limit of PSR J1648–4611

Since the X-ray emission of PSR J1648–4611 was not detected by the point source search for the Chandra image, we estimated the intensity upper limit using the Chandra data as follows. The event number in the 0.4–10 keV band in a circular region with a radius of $3''$ centered on the pulsar is 3 counts. We set the source region larger than the point spread function

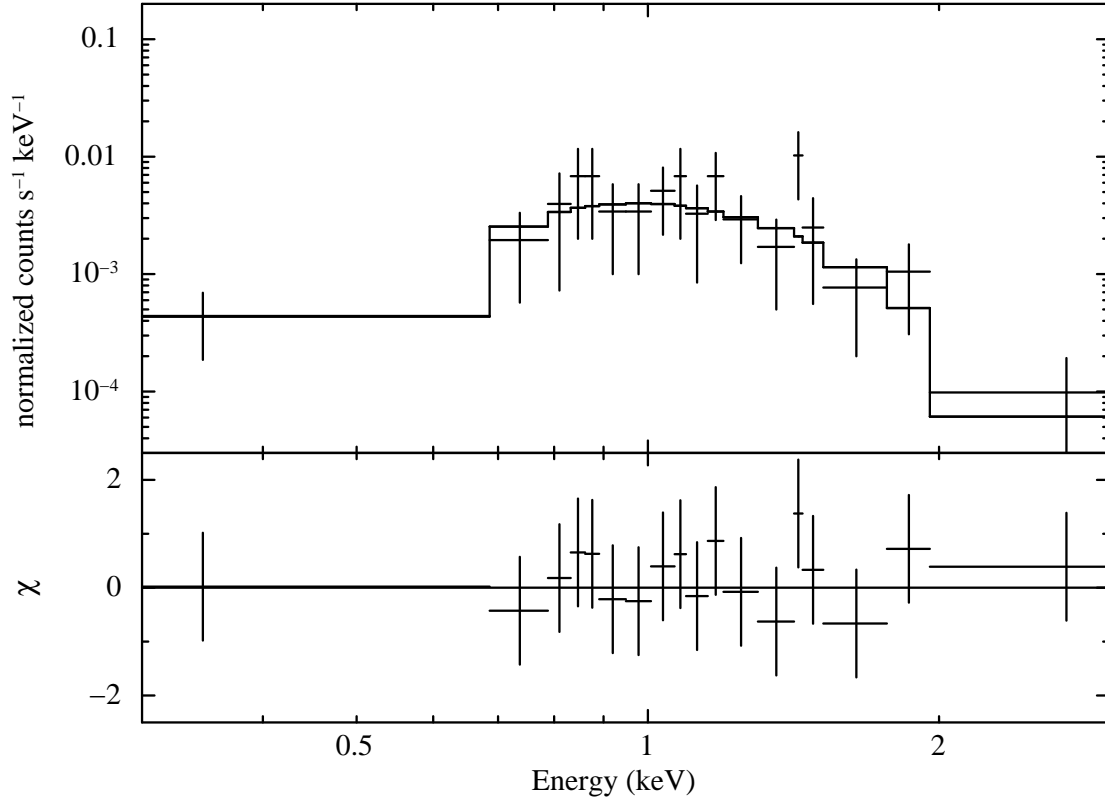


Fig. 5. Combined Chandra spectrum of three point sources (Srcs 1, 2 and 3). Black lines represent the best-fit model.

of Chandra to include the possible extended emission from a compact PWN (Kargaltsev et al. 2012). A background was estimated using an annular region with an inner radius of $2'$ and an outer radius of $3'$, which was outside of the Suzaku Src A region, and the background event number in the 0.4–10 keV band was 1300; the event number normalized to the source region was 0.65 counts. The event number in the source region after subtracting the background was estimated to be $2.35^{+3.01}_{-2.05}$ counts by a numerical simulation assuming the Poisson statistics; since the 99% confidence range was estimated to be $2.35^{+4.01}_{-3.02}$ counts and was consistent with zero, we conservatively think that the X-rays from the pulsar is not statistically significant. The upper limit on the pulsar X-rays in the 0.4–10 keV band at the 90% confidence level was thus 5.4 counts. The count number was converted to the energy flux in the 0.4–10 keV band by using webPIMMS⁸ assuming a power-law model with $\Gamma = 2$ and a hydrogen column of $N_{\text{H}} = 2 \times 10^{22} \text{ cm}^{-2}$ where we adopted the total Galactic HI column density towards PSR J1648–4611 (Dickey & Lockman 1990). The upper limit on the X-ray flux of PSR J1648–4611 in the 0.4–10 keV band was thus calculated to be $1.0 \times 10^{-14} \text{ erg s}^{-1} \text{ cm}^{-2}$, while that on the unabsorbed flux

⁸ (<http://heasarc.gsfc.nasa.gov/Tools/w3pimms.html>).

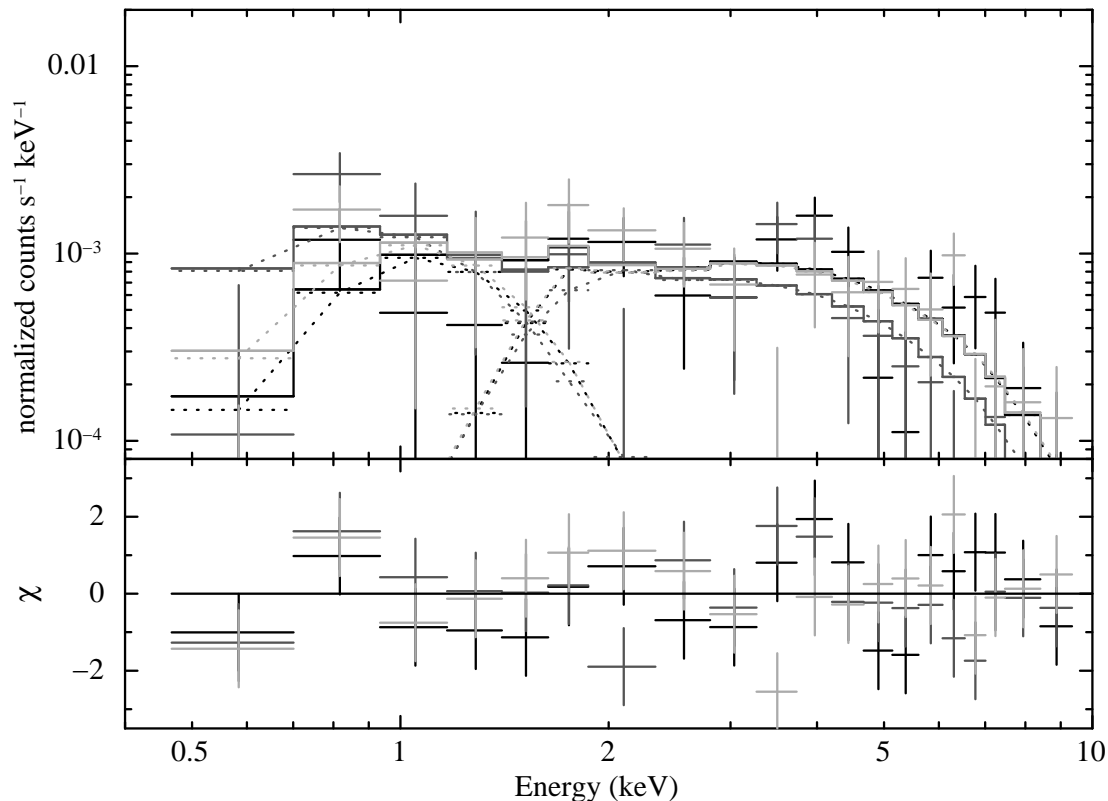


Fig. 6. XIS spectra of Src A. Black, Dark Gray and Light Gray lines represent the data and model for the XIS0, XIS1 and XIS3, respectively. The contribution of Chandra point sources is indicated by the dotted lines in the soft-band. The additional dotted lines in the hard-band show the diffuse component.

was $2.3 \times 10^{-14} \text{ erg s}^{-1} \text{ cm}^{-2}$.

4. Discussion

4.1. X-ray emission from PSR J1648–4611

The X-ray emission from the pulsar PSR J1648–4611 was not detected in the Chandra image. The upper limit on the flux of PSR J1648–4611 yields the upper limit on the luminosity of $8.8 d_{5.7}^2 \times 10^{31} \text{ erg s}^{-1}$ in the 0.4–10.0 keV band, where $d_{5.7}$ is the distance scaled to 5.7 kpc.

Kargaltsev et al. (2012) also analyzed the same Chandra data and detected no X-rays from the pulsar. Their upper limit on the X-ray count in the 0.4–10 keV band in the circular region with a radius of $3''$ is, however, 3.1 counts, which we converted from their upper limit on the X-ray flux in the 0.5–8 keV band ($5.2 \times 10^{-15} \text{ erg s}^{-1} \text{ cm}^{-2}$) using their assumed model (a power-law model of $\Gamma = 1.5$ and $N_{\text{H}} = 1.2 \times 10^{22} \text{ cm}^{-2}$). This value is only $\sim 60\%$ of our estimate. The main reason for the discrepancy is the difference of the methods for the upper limit;

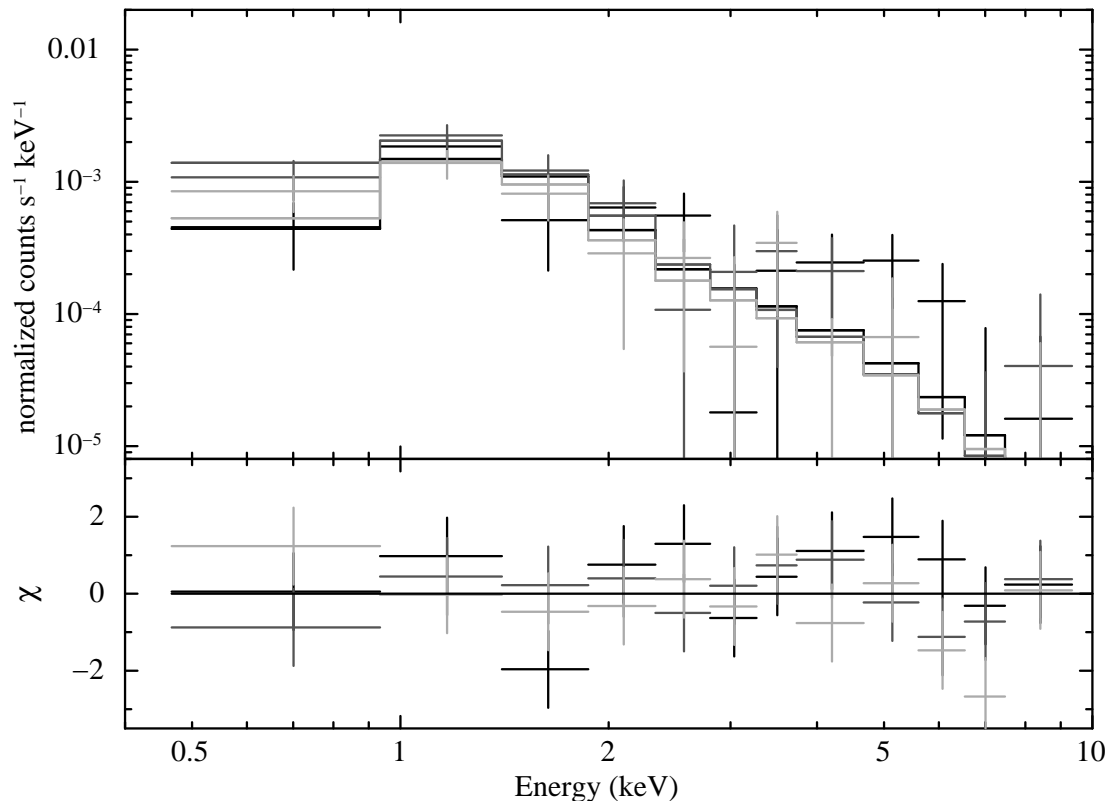


Fig. 7. XIS spectra of Src B. Black, Dark Gray and Light Gray lines represent the data and model for the XIS0, XIS1 and XIS3, respectively.

Kargaltsev et al. (2012) estimated the upper limit only from the background event number, while we obtained it using both the source and background event numbers. Our value is conservative anyway.

The upper limit on the X-ray luminosity in the 0.1–2.4 keV band is $8.7 d_{5.7}^2 \times 10^{31} \text{ erg s}^{-1}$. Following the relation between the spin-down power and X-ray luminosity of rotation-powered pulsars (Becker & Trümper 1997), the expected X-ray luminosity of PSR J1648–4611 in the 0.1–2.4 keV band would be $L_X \sim 10^{32} \text{ erg s}^{-1}$. This value is consistent with our upper limit. Since pulsed GeV emission with the rotation period of PSR J1648–4611 is observed with the Fermi satellite,⁹ it is natural to expect an X-ray emission of the pulsar. However, even if PSR J1648–4611 would have X-ray emission with the luminosity expected from the spin-down luminosity, we would not be able to detect it with the short exposure time (~ 10 ks) because of the heavy extinction due to the Galactic plane and of the distance.

⁹ See <https://confluence.slac.stanford.edu/display/GLAMCOG/Public+List+of+LAT-Detected+Gamma-Ray+Pulsars>.

4.2. Diffuse hard X-ray emission from Src A

We found the diffuse hard X-ray emission from Src A in the Suzaku image. The peak position of the emission is close to PSR J1648–4611. A natural interpretation is that the diffuse hard X-ray emission comes from a PWN around PSR J1648–4611. The photon index of the hard X-ray emission is $2.0_{-0.7}^{+0.9}$. This value is consistent with the typical values of PWNe (Fleishman & Bietenholz 2007 and references therein). The column density $N_{\text{H}} = 3.4_{-1.6}^{+2.4} \times 10^{22} \text{ cm}^{-2}$ is also consistent with the Galactic HI column density towards PSR J1648–4611 ($\sim 2 \times 10^{22} \text{ cm}^{-2}$; Dickey & Lockman 1990). Furthermore, a constant component in the GeV emission is reported (Abramowski et al. 2012), and the component also suggests the existence of the PWN.

On the other hand, the luminosity of the diffuse hard X-ray emission is $7.3 d_{5.7} \times 10^{32} \text{ erg s}^{-1}$ in the 2–10 keV band. Following the relation between spin-down power/characteristic age and X-ray luminosity of PWNe (Mattana et al. 2009), the expected X-ray luminosity of the associated PWN would be $L_{\text{X}} \sim 10^{31} \text{ erg s}^{-1}$. Thus our result is much larger than the expected luminosity, even when the uncertainty in the distance estimation of $\sim 30\%$ (Kramer et al. 2003) is taken into account. Furthermore we obtained the lower limit on the ratio of the PWN to pulsar luminosities $L_{\text{PWN}(0.5-8\text{keV})}/L_{\text{PSR}(0.5-8\text{keV})} \geq 16$. This value is larger than the average $L_{\text{PWN}(0.5-8\text{keV})}/L_{\text{PSR}(0.5-8\text{keV})} \sim 4$ reported by Kargaltsev et al. (2007). Additionally, the physical size of the diffuse X-ray emission is $\sim 3.3 d_{5.7}(\theta/2')\text{pc}$, where θ is the angular radius of Src A. This size is an order of magnitude smaller than the expected value based on the PWN size-age relation reported by Bamba et al. (2010). Therefore if the diffuse hard X-ray emission is the PWN of PSR J1648–4611, it is much brighter than that expected from the spin-down luminosity of the pulsar, and the spatial extension is rather compact.

4.3. Connection to HESS J1646-458

If the origin of the TeV emission from HESS J1646–458 is PSR J1648–4611, an unreasonably high efficiency of $\epsilon_{\gamma} = L_{\gamma}/\dot{E} = 96 d_{5.7}^2\%$ is required for the production of TeV flux of HESS J1646–458, which is $5.2 \times 10^{-11} \text{ cm}^{-2} \text{ s}^{-1}$ above 0.2 TeV (Abramowski et al. 2012). Additionally, the observed VHE γ -ray emitting region has a diameter of about 2° , which is a factor of ~ 30 larger than that of the X-ray emitting region of Src A and is not consistent with the ratio between the predicted VHE γ -ray and X-ray size of PWN (~ 6 : Aharonian et al. 2005). These results imply that HESS J1646–458 seems unlikely to be explained only as a PWN powered by PSR J1648–4611. However, it is conceivable that parts of the VHE γ -ray emission of HESS J1646–458 are powered by the pulsar.

5. Summary

We observed the pulsar PSR J1648–4611 with Suzaku, and discovered the diffuse hard X-ray emission around PSR J1648–4611. The spatial distribution and the photon index of the

diffuse emission suggest that a PWN exists around the pulsar. The luminosity of the diffuse emission, however, is much larger than that expected from the spin-down luminosity of the pulsar. Parts of the VHE γ -ray emission of HESS J1646–458 could be caused by this PWN powered by PSR J1648–4611.

We are grateful to H. Kunieda, and H. Mori for their useful comments. We would like to thank all Suzaku members. MS is supported by Grant-in-Aid for Japan Society for the Promotion of Science (JSPS) Fellows, 23-5737, HM is supported by Grant-in-Aid for Scientific Research (B), 22340046. This work is partially supported by the Grant-in-Aid for Nagoya University Global COE Program, “Quest for Fundamental Principles in the Universe: from Particles to the Solar System and the Cosmos”, from the Ministry of Education, Culture, Sports, Science and Technology of Japan.

References

- Abramowski, A., et al. 2012, *A&A*, 537, A114
Aharonian, F., et al. 2005, *A&A*, 442, L25
Bamba, A., Anada, T., Dotani, T., Mori, K., Yamazaki, R., Ebisawa, K., & Vink, J. 2010, *ApJL*, 719, L116
Becker, W., & Trümper, J. 1997, *A&A*, 326, 682
Dickey, J. M., & Lockman, F. J. 1990, *ARA&A*, 28, 215
Fleishman, G. D., & Bietenholz, M. F. 2007, *MNRAS*, 376, 625
Freeman, P. E., Kashyap, V., Rosner, R., & Lamb, D. Q. 2002, *ApJS*, 138, 185
Ishisaki, Y., et al. 2007, *PASJ*, 59, S113
Kargaltsev, O., Pavlov, G. G., & Garmire, G. P. 2007, *ApJ*, 660, 1413
Kargaltsev, O., Durant, M., Pavlov, G. G., & Garmire, G. 2012, *ApJS*, 201, 37
Kokubun, M., et al. 2007, *PASJ*, 59, S53
Koyama, K., et al. 2007, *PASJ*, 59, S23
Kramer, M., et al. 2003, *MNRAS*, 342, 1299
Mattana, F., et al. 2009, *ApJ*, 694, 12
Mitsuda, K., et al. 2007, *PASJ*, 59, 1
Morrison, R., & McCammon, D. 1983, *ApJ*, 270, 119
Nolan, P. L., et al. 2012, *ApJS*, 199, 31
Serlemitsos, P. J., et al. 2007, *PASJ*, 59, S9
Smith, R. K., Brickhouse, N. S., Liedahl, D. A., & Raymond, J. C. 2001, *ApJ*, 556, L91
Takahashi, T., et al. 2007, *PASJ*, 59, S35
Tawa, N., et al. 2008, *PASJ*, 60, S11
Taylor, J. H., & Cordes, J. M. 1993, *ApJ*, 411, 674
Uchiyama, H., et al. 2009, *PASJ*, 61, S9
Westerlund, B. 1961, *AJ*, 66, 57